group $m\bar{3}\bar{5}$, as opposed to 235 (noncentrosymmetric). The reasons for this choice of point group are explained by the authors in terms of transmission electron microscopy (TEM) analysis. No inversion domains could be found in TEM images of Al–Cu–Fe samples [Rzepski, Quivy, Calvayrac, Cornier-Quiquandon & Gratias (1989), § 3; Cornier-Quiquandon, Quivy, Lefèbvre, Elkaim, Heger, Katz & Gratias (1991), footnote 36]. In other words, no convincing evidence of lack of centrosymmetry was found and centrosymmetry could not be ruled out altogether.

In conclusion, we have demonstrated the feasibility of phasing structure factors in a quasicrystal with use of multiple Bragg scattering. The phase values for the triplet invariants obtained by this method are model independent and can be used to assess different structural models.

Special thanks are due to P. Bancel who provided the material used in this work and offered invaluable technical assistance in understanding the physics of quasicrystals. The authors are indebted to V. Elser for several extensive discussions. The generous help of S. Ehrlich and X. Yang of NSLS and J. Arthur of SSRL in recording the synchrotron data is deeply appreciated. Thanks are also due to D. Gratias for many illuminating discussions on basic issues of quasicrystallography.

This work was supported by NSF Grant DMR-8715503 and by a DOE Grant DE-FG02-85ER45183, which supports the operations of beamline X-18A at NSLS.

References

BERENSON, R. & BIRMAN, J. L. (1986). *Phys. Rev. B*, **34**, 8926–8928.
CHANG, S. L. (1987). *Crystallogr. Rev.* **1**, 87–184.
CHANG, S. L., KING, H. E. JR, HUANG, M. T. & GAO, Y. (1991). *Phys. Rev. Lett.* **67**, 3113–3116.
CHAPMAN, L. D., YODER, D. R. & COLELLA, R. (1981). *Phys. Rev. Lett.* **46**, 1578–1581.
COLELLA, R. (1974). *Acta Cryst.* A**30**, 413–423.
COLELLA, R. (1982). *Z. Naturforsch. Teil A*, **37**, 437–447.
CORNIER-QUIQUANDON, M., QUIVY, A., LEFÈBVRE, S., ELKAIM, E., HEGER, G., KATZ, A. & GRATIAS, D. (1991). *Phys.*
ELSER, V. (1986). *Acta Cryst.* A**42**, 36–43, Appendix, § 2, equations (21) and (23).
ELSER, V. (1991). Private communication.
HÜMMER, K., SCHWEGLE, W. & WECKERT, E. (1991). *Acta Cryst.* A**47**, 60–62.
JANOT, C., PANNETIER, J., DE BOISSIEU, M. & DUBOIS, J. M. (1987). *Europhys. Lett.* **3**, 995–1000.
RZEPSKY, J. D., QUIVY, A., CALVAYRAC, Y., CORNIER-QUIQUANDON, M. & GRATIAS, D. (1989). *Philos. Mag.* B**60**, 855–869.
SHEN, Q. (1986). *Acta Cryst.* A**42**, 525–533.
SHEN, Q. & COLELLA, R. (1987). *Nature (London)*, **329**, 232–233.
TISCHLER, J. Z., SHEN, Q. & COLELLA, R. (1985). *Acta Cryst.* A**41**, 451–453.

Acta Cryst. (1993). A**49**, 605–613

Effects of a General X-ray Polarization in Multiple-Beam Bragg Diffraction

BY QUN SHEN

Cornell High-Energy Synchrotron Source (CHESS) and Department of Applied Engineering Physics, Cornell University, Ithaca, New York 14853, *USA*

(*Received* 12 *October* 1992; *accepted* 22 *December* 1992)

Abstract

The formalism of the *N*-beam dynamical theory of X-ray diffraction is extended to include all possible incident and diffracted polarizations. With this new formalism it is shown that the intensity of a simultaneously excited Bragg reflection can be described through a polarization density matrix that involves the Stokes–Poincaré parameters. In particular, the multibeam diffracted intensity is sensitive to the circularly polarized component in the incident beam and the structure-factor phases of the diffracting crystal. Experimental results on the GaAs 442 and Ge 333 reflections confirm the theoretical calculations. This kind of measurement can provide useful acentric phase information and can also be used for circular X-ray polarimetry. Another feature of *N*-beam diffraction is its ability to turn a linear polarization into an elliptical polarization, which means it can be used as an X-ray phase plate.

Introduction

X-ray polarization plays an important role in every scattering and diffraction experiment. In crystallography, one needs to use the polarization-factor correction in order to obtain structure factors from diffracted intensities (Warren, 1969). In X-ray physics and

material science, polarization analysis can often reveal interesting features of the magnetic properties and atomic-site symmetries of the diffracting material (Templeton & Templeton, 1985; Blume & Gibbs, 1988; Belyakov & Dmitrienko, 1989; Kirfel, Petcov & Eichhorn, 1991; Finkelstein, Shen & Shastri, 1992). The increasingly available energy and polarization tunabilities of many intense synchrotron sources promise to provide experimenters with an extra dimension in the analysis of X-ray polarization in future diffraction experiments. It is, therefore, worthwhile to re-examine and extend some of the well established fields in X-ray diffraction. One such field is that of multiple-beam Bragg diffraction. Because of the co-existing effects of *multibeam interference* and *polarization mixing* (Shen, 1991), some new and interesting features in multibeam diffraction can emerge if one includes general elliptically polarized X-rays in the incident beam. These new features include phase determination on noncentrosymmetric crystals (Shen & Finkelstein, 1990), complete characterization of an elliptical polarization of an X-ray beam (Shen & Finkelstein, 1992) and utilization of multibeam diffraction as an X-ray circular phase plate.

Multiple-beam diffraction occurs in a crystal when two or more atomic planes satisfy the Bragg conditions simultaneously. The process usually gives rise to a secondary peak (Renninger peak) in the intensity of a Bragg reflection, **H**, when the diffraction crystal is rotated around the scattering vector **H** (Renninger, 1937; Cole, Chambers & Dunn, 1962). The reflection **H** is usually termed the main reflection and the rotation is described by an azimuthal angle, φ. Throughout this article, we use the convention that the symbol **H**/**L** refers to a multiple-beam situation with the Renninger reflection **L** on the main reflection **H**. Theoretical investigations of multiple-reflection intensities have been extensive, ranging from an energy-balancing kinematical approach (Moon & Shull, 1964; Zachariasen, 1965) to a full N-beam dynamical theory formalism, developed by Colella (1974). The main purpose of this article is to incorporate a density-matrix representation into Colella's (1974) formalism, so that multiple-beam dynamical calculations can be performed in a straightforward way for any incident-beam polarization. It also allows for convenient calculations of the scattered polarization in a multibeam diffraction process. Applications of the new formalism are presented in several examples and are compared with experimental results obtained using elliptically polarized synchrotron radiation.

The dynamical theory of X-ray diffraction calculates a diffracted intensity in two steps (Batterman & Cole, 1964). First, it solves an eigenvalue equation to obtain all the possible wave vectors that can exist inside the crystal; the result is the so-called dispersion surface. Second, it matches the boundary conditions at the crystal surface to calculate the relative amplitudes of the possible wavefields inside and outside the crystal for a given incident-beam direction $\mathbf{k}_0$ and polarization $\mathbf{D}_0$. In general, both the incident and the diffracted wavefields, $\mathbf{D}_0$ and $\mathbf{D}_H$, outside the crystal can be decomposed into polarization directions perpendicular (σ) and parallel (π) to the scattering plane defined by $\mathbf{k}_0$ and **H**. The procedure is the same in the general N-beam case as in the two-beam case. The key result of the N-beam dynamical theory is that the diffracted wavefield $\mathbf{D}_H$ now depends upon other inside wavefields, say, **L**, rather than just upon the incident **O** and the diffracted **H** waves as in the two-beam case.

The computational procedure in the case of N beams is extensive, as one might imagine. One needs to diagonalize a $4N \times 4N$ eigenvalue matrix in the first step and to solve a $4N$ linear equation system in the second step. Fortunately, both problems have been solved in Colella's (1974) formalism. To generalize for an arbitrary incident polarization, one only needs to calculate a 2×2 matrix, $\{\mathbf{M}\}$, using Colella's formalism, that relates the incident **O** beam ($D_{0\sigma}$, $D_{0\pi}$) and the main reflected **H** beam ($D_{H\sigma}$, $D_{H\pi}$) outside the crystal. The matrix $\{\mathbf{M}\}$ contains four complex numbers, $M_{\sigma\sigma}$, $M_{\pi\sigma}$, $M_{\sigma\pi}$ and $M_{\pi\pi}$, representing the $\sigma \rightarrow \sigma$, $\pi \rightarrow \sigma$, $\sigma \rightarrow \pi$ and $\pi \rightarrow \pi$ diffracted wavefields, respectively.

$$\begin{bmatrix} D_{H\sigma} \\ D_{H\pi} \end{bmatrix} = \begin{bmatrix} M_{\sigma\sigma} & M_{\pi\sigma} \\ M_{\sigma\pi} & M_{\pi\pi} \end{bmatrix} \begin{bmatrix} D_{0\sigma} \\ D_{0\pi} \end{bmatrix}. \quad (1)$$

The possible existence of the off-diagonal matrix elements in $\{\mathbf{M}\}$ indicates that the polarization states can be mixed in a multiple-beam diffraction process (Shen & Finkelstein, 1992).

Although (1) can accommodate all pure incident-beam polarizations, it is inconvenient to calculate the diffracted intensity if the incident beam is partially polarized. The best way to overcome this difficulty is to define the incident polarization with a density matrix, $\{\boldsymbol{\rho}\}$. As we know, in optics, the intensity and polarization of any electromagnetic plane wave, $\mathbf{D} = (D_\sigma, D_\pi e^{i\varepsilon})$, can be completely characterized by the four Stokes parameters (Born & Wolf, 1983): $s_0 = D_\sigma^2 + D_\pi^2$, $s_1 = D_0^2 - D_\pi^2$, $s_2 = 2D_0 D_\pi \cos\varepsilon$ and $s_3 = 2D_\sigma D_\pi \sin\varepsilon$, which represent the total intensity, the intensity difference between the 0 and the 90° polarizations, the intensity difference between the 45 and the $-45°$ linear polarizations and the intensity difference between the right- and the left-handed circular polarizations, respectively. If one is interested only in the polarization aspect then one can use the normalized Stokes parameters: $(P_1, P_2, P_3) = (s_1, s_2, s_3)/s_0$. The vector $\mathbf{P} = (P_1, P_2, P_3)$ is called the

Poincaré vector of polarization. Any X-ray plane wave can be represented by a vector **P** which defines a point in Poincaré space (Fig. 1). A completely polarized beam corresponds to a point on the Poincaré sphere $|\mathbf{P}|=1$, while partially polarized beams correspond to the points within the sphere ($|\mathbf{P}|<1$). A polarization density matrix, $\{\boldsymbol{\rho}\}$, for a given incident X-ray polarization $\mathbf{P}=(P_1, P_2, P_3)$ is defined by

$$\{\boldsymbol{\rho}\}=\tfrac{1}{2}\begin{bmatrix} 1+P_1 & P_2-iP_3 \\ P_2+iP_3 & 1-P_1 \end{bmatrix}. \tag{2}$$

When the incident X-rays are scattered or diffracted by $\{\mathbf{M}\}$, its polarization **P** and thus $\{\boldsymbol{\rho}\}$ change in the following way:

$$\{\boldsymbol{\rho}'\}=\{\mathbf{M}\boldsymbol{\rho}\mathbf{M}^{\dagger}\}, \tag{3}$$

where $\{\boldsymbol{\rho}'\}$ is the density matrix of the diffracted beam and the superscript dagger indicates the Hermitian conjugate. The diffracted intensity, I, is expressed by the trace of the new density matrix (Blume & Gibbs, 1988):

$$I=\mathrm{Tr}\{\boldsymbol{\rho}'\}. \tag{4}$$

To summarize the above discussion, an N-beam dynamical calculation with a general incident-beam polarization proceeds as follows: (i) Calculate the 2×2 matrix $\{\mathbf{M}\}$ using Colella's *NBEAM* program (Colella, 1974). This step involves four independent calculations, of the $\sigma\rightarrow\sigma$, $\pi\rightarrow\sigma$, $\sigma\rightarrow\pi$ and $\pi\rightarrow\pi$ diffracted wavefields. (ii) Define a density matrix $\{\boldsymbol{\rho}\}$ with the polarization parameters (P_1, P_2, P_3) that characterize the incident X-ray beam. (iii) Calculate the diffracted intensity using (3) and (4). A version of Colella's original *NBEAM* program has been modified to include all three steps and the new program is named *NBEAM-MTRX.*

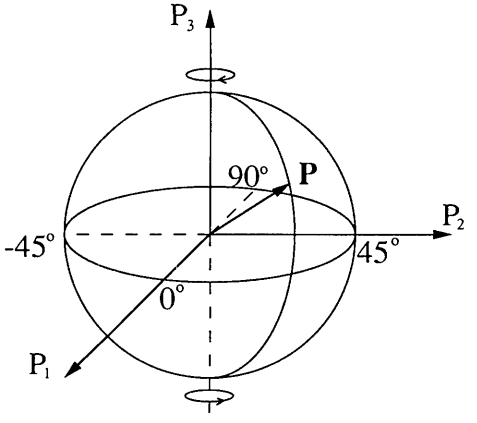

Fig. 1. Poincaré representation of X-ray polarization. Any polarization of an X-ray beam can be specified by a vector $\mathbf{P}=(P_1, P_2, P_3)$ in Poincaré space. In general, $|\mathbf{P}|\leq 1$, with the equality corresponding to a completely polarized beam and the inequality to a partially polarized one.

Applications of the new formalism

The new *NBEAM-MTRX* formalism provides a useful tool for doing multiple-beam dynamical diffraction calculations with a general incident polarization. We show three examples of the application of the new formalism and make comparisons with experiments using elliptically polarized synchrotron radiation.

1. GaAs 442: *solving acentric phase problems*

It has been known that the interference effect in a multiple-beam diffraction process can be used to extract lost crystallographic phase information from diffraction intensities (Colella, 1974; Post, 1977; Chapman, Yoder & Colella, 1981; Chang, 1982; Juretschke, 1982; Shen, 1986; Shen & Colella, 1986; Hummer & Billy, 1986; Shen & Colella, 1987, 1988; Chang & Tang, 1988; Hummer, Weckert & Bondza, 1989; Shen & Finkelstein, 1990). As realized by several authors, when linearly polarized or unpolarized X-rays are used as the incident beam, the multi-beam interference effect on the wings of a multiple reflection peak contains information on only the cosine of the relative phase or the real part of the phase factor. The information on the sine of the relative phase, which is directly related to the non-centrosymmetry of a crystal, is still missing in such an experiment. Although such phase information may exist at the center of a multiple-reflection peak (Hummer & Billy, 1986; Chang & Tang, 1988; Hummer, Weckert & Bondza, 1989), it is usually affected by the kinematic effect if one uses the dynamical theory or the extinction effect if one uses the kinematic theory. Recently it has been demonstrated by Shen & Finkelstein (1990) that another way to obtain the noncentrosymmetric phase information is to utilize circularly polarized X-rays as the incident beam in a multiple-beam diffraction experiment. Because of the polarization mixing and the interference between complex polarization and complex phase factors, the interference intensity on the wings of the multiple-reflection peak will depend upon both the real and imaginary parts of the phase factor.

As an example to illustrate an N-beam dynamical calculation and to compare it with the results of an experiment, we repeat the calculation that was carried out in our earlier publication with the new *NBEAM-MTRX* formalism and compare the result with our experimental data. The experiment was performed at a bending magnet station, D1, at the Cornell High-Energy Synchrotron Source (CHESS). The station was equipped with a double-bounce Si (111) monochromator diffracting in the vertical plane and was tuned to 1.3 Å X-ray wavelength. In the experiment, we measured three-beam diffraction profiles

on a GaAs 442 main reflection using elliptically polarized (Jackson, 1975) synchrotron radiation above and below the electron (position) orbital plane. The GaAs crystal surface was parallel to the (111) atomic planes. Fig. 2 shows the three-beam profiles around the 442/151 multiple reflection, with (*a*) left-handed elliptical polarization at 0.11 mrad above and (*b*) right-handed elliptical polarization at 0.11 mrad below the orbital plane. Each data point is an integrated intensity over a 442 rocking curve. GaAs is a noncentrosymmetric polar crystal. In a given diffraction geometry the GaAs can have an atomic arrangement with either the Ga atoms at the $+(1/8, 1/8, 1/8)$ sites and As atoms at the $-(1/8, 1/8, 1/8)$ sites, or an arrangement with the Ga atoms at the $-(1/8, 1/8, 1/8)$ sites and As atoms at the $+(1/8, 1/8, 1/8)$ sites. The first situation corresponds to a phase triplet $\delta \simeq +90°$ for the 442/151 multiple reflection and the second case to a phase $\delta \simeq -90°$.

A three-beam dynamical calculation is performed on the GaAs 442/151 reflection using the new *NBEAM-MTRX* program and the results are shown in Figs. 2 and 3. The solid curves in Fig. 2 are integrated intensities using $\delta \simeq +90°$ and the dashed curves are those obtained with $\delta \simeq -90°$. The polarization of the incident beam is assumed to be $\mathbf{P} =$

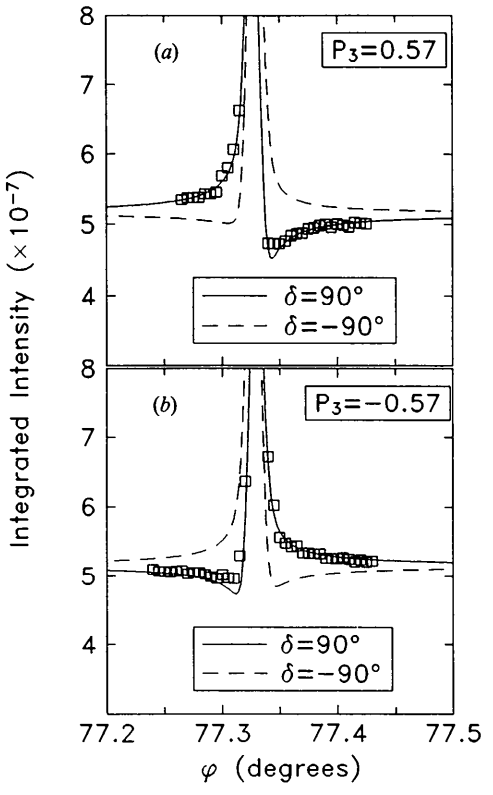

Fig. 2. Three-beam interference intensity profiles of GaAs 442/151 using elliptically polarized synchrotron radiation (*a*) above and (*b*) below the orbital plane. The experimental data are shown as squares. The curves shown are three-beam dynamical calculations using $\delta = 90°$ (solid curve) and $\delta = -90°$ (dashed curve). The incident polarization used in the calculation is $\mathbf{P} = (0.77, 0, 0.57)$ in (*a*) and $\mathbf{P} = (0.77, 0, -0.57)$ in (*b*), which are consistent with the synchrotron-radiation properties and the experimental conditions. The azimuthal-angle origin is defined by the convention that the reciprocal vector $(-1, 1, 0)$ is lying on the diffraction plane, with a projection that is antiparallel to the incident wave vector $\mathbf{k}_0$. The surface normal of the crystal is along the [111] direction.

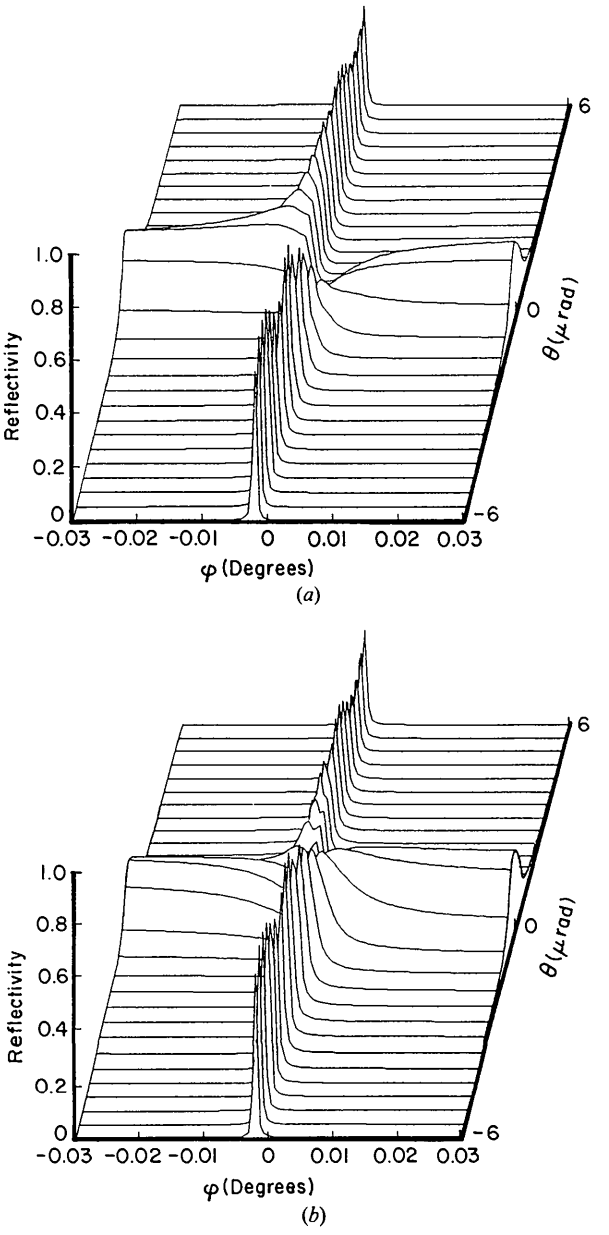

Fig. 3. Calculated reflectivity of the GaAs 442/151 multiple reflection as a function of rocking-curve angle θ and azimuthal angle φ. The incident polarization is assumed to be (*a*) $\mathbf{P} = (0.77, 0, 0.57)$ and (*b*) $\mathbf{P} = (0.77, 0, -0.57)$. The definitions of the zero points on both the θ and φ axes are arbitrary.

(0.77, 0, 0.57) above the orbital plane and $\mathbf{P}=$ (0.77, 0, −0.57) below the orbital plane. These values of the polarization parameters have been derived from three multiple-beam diffraction profiles measured in an experiment and the procedure has been discussed elsewhere (Shen & Finkelstein, 1992). Fig. 2 shows very good agreement between the theory and the experiment and indicates unambiguously that the correct relative phase δ is +90° for our diffraction geometry. This demonstrates that a circularly polarized X-ray beam can be utilized to provide acentric phase information through a multiple-beam diffraction process.

Figs. 3(*a*) and (*b*) show the results of *NBEAM-MTRX* calculations for the GaAs 442 reflection as functions of both the azimuthal angle φ and the rocking angle θ near the 151 multiple reflection. The incident polarization is $\mathbf{P}=(0.77, 0, 0.57)$ for Fig. 3(*a*) and $\mathbf{P}=(0.77, 0, -0.57)$ for Fig. 3(*b*). The plots are very informative in illustrating the behavior of the asymmetric intensity profiles caused by multiple-beam excitation. There are basically two ridges of high reflectivities, running parallel to the φ axis and the θ axis, respectively. The one parallel to the φ axis (independent of φ) is caused by the main reflection 442 and the other is due to the 151 multiple reflection. As expected, the greatest interference between them occurs where these two ridges meet. Asymmetric reflectivity profiles should exist in both the φ and θ directions, but the φ dependence extends to ~0.01°, which is about 100 times broader than the θ dependence. Therefore, it should be much easier to observe an asymmetry pattern in an azimuthal scan. We may also note that the θ range shown in Fig. 3 is much smaller than the incident-beam divergence under typical experimental conditions (~100 μrad in our experiment). Thus the θ-integrated intensity comes out naturally in an experiment even without rocking θ. As Fig. 3 shows, only in the θ-integrated intensity will a strong peak at $\varphi=0$ appear, because of the long and strong ridge due to the multiple reflection.

Fig. 3 clearly shows that the intensity asymmetry along the main reflection ridge (parallel to the φ axis) is reversed when the handedness of the elliptical polarization is switched. Since this effect occurs outside the full excitation width of the multiple reflection, and the main reflection, GaAs 442, is relatively weak, one can apply a perturbation theory based on kinematic scattering to fully explain the multiple-beam interference effect (Shen, 1986). With the use of such a perturbation theory, it is straightforward to show that the circular polarization effect in the multi-beam interference intensity on the wings of a multiple reflection depends exclusively on the sine of the three-beam phase triplet δ (Shen & Finkelstein, 1992):

$$I_{\text{circular}} \propto (-M_{\pi\sigma} + M_{\sigma\pi} \cos 2\theta) \sin \delta P_3, \quad (5)$$

where $M_{\pi\sigma}$ and $M_{\sigma\pi}$ are the off-diagonal elements of $\{\mathbf{M}\}$ defined in (1), θ is the Bragg angle of the main reflection $\mathbf{H}$ and P_3 is the purity of the circular polarization of the incident beam. Equation (5) implies that, with a known crystal structure and, therefore, a known δ, one can use the same multibeam interference effect to measure the degree of circular polarization of an X-ray beam, as discussed in earlier publications.

2. *Germanium* 333: *strong main reflection*

On the sides of a multiple reflection peak, either the *N*-beam dynamical theory (Colella, 1974) or the modified two-beam perturbation theory (Juretschke, 1982; Shen, 1986) can be applied to calculate the multiple-beam interference. At the center of a multiple-reflection peak, however, the perturbational approaches fail and a full *N*-beam calculation is usually required. In this section such a calculation on the Ge 333 reflection is shown and the results are compared with experimental measurements.

Equation (5) reveals that, in order for the circular polarization dependence in the neighborhood of a multiple reflection to be observed, a noncentrosymmetric crystal is necessary to provide a nonzero sin δ, if anomalous dispersion is ignored. On the other hand, it is well known that by sweeping through the full excitation width of any Bragg reflection, the diffracted wave field changes in phase from 0 to π relative to the incident beam *in addition* to undergoing the kinematic phase shift due to the structure factor (Bedzyk & Materlik, 1985). This implies that there should exist a phase variation, $\nu(\varphi)$, within the range of full excitation of a multiple reflection, that provides nonvanishing $\sin[\delta+\nu(\varphi)]$ even for a centrosymmetric crystal (where δ can be only 0 or π). For centrosymmetric crystals, therefore, the diffracted intensity near the center of a multiple reflection should be sensitive to circular polarization in the incident beam.

Fig. 4 shows the calculated Ge 333/13$\bar{3}$ multiple-beam reflectivities as a function of the 333 rocking-curve angle θ and its azimuthal angle φ, with right-handed circular polarization $\mathbf{P}=(0, 0, 1)$ in Fig. 4(*a*) and left-handed polarization $\mathbf{P}=(0, 0, -1)$ in Fig. 4(*b*). The results appear very different from the case of GaAs 442/151, in several ways. First, the main-reflection rocking curve is much wider than that of the GaAs 442 because Ge 333 is a much stronger reflection. Second, the ridge due to the multiple reflection, 13$\bar{3}$, is weak outside the main-reflection rocking curve because the 13$\bar{3}$ is a reflection with a similar strength to the 333. Third, the multibeam interaction occurs in a range of azimuthal angles that is comparable to the rocking-curve width of the main reflection, whereas in the case of GaAs 442 the interaction extends to a

range that is hundreds of times wider than the 442 rocking width. The reason for this is that the weak 442 wavefield can interfere with the weakly excited strong reflection 151 and the maximum interference should occur at the azimuthal angles where the 442 and the 151 wavefields have similar strengths.

Despite the differences between Figs. 3 and 4, Figs. 4(*a*) and (*b*) do exhibit a distinct difference in reflectivity when the sense of the polarization handedness is switched. The circular handedness also strongly affects the θ-integrated intensities, which are shown in Fig. 5. As one can see, the two intensity profiles in Fig. 5 do not resemble the sense of asymmetry reversal as in the case of GaAs 442/151 multiple reflection in Fig. 2. This difference can again be explained by the strengths of the main reflections. The Ge 333 is a strong reflection and, therefore, has a well defined dynamical phase change of π within its excitation width. It is this phase change that biases the asymmetry in the interference intensity. The GaAs 442, on the other hand, is a relatively weak reflection and is more kinematically excited. Its intrinsic rocking-curve width is only ~ 1.3 μrad, compared to ~ 18 μrad in the case of Ge 333. Therefore, the dynamical phase change for the GaAs 442 is not well defined and plays a much lesser role in the three-beam interference. The effect is then dominated by the phase change of the multiple reflection 151 which causes the interference intensity that can be correctly described by (5).

To confirm the circular polarization dependence of the Ge 333/13$\bar{3}$ reflection, we performed an experiment at the CHESS D1 station, using the elliptically polarized off-orbital plane radiation. The station for this experiment was set up with a single-crystal horizontal diffracting Si (111) monochromator preceded by a total reflecting mirror. The monochromator provided 1.5 Å X-rays incident on the germanium sample. The measurement of three-beam diffraction profiles on the 333/13$\bar{3}$ were obtained above and below the orbital plane where the incident synchrotron radiation is ~90% circularly polarized $\mathbf{P} = (0.43, 0, \pm 0.90)$, according to a calculation based on synchrotron properties. The measured intensity profiles, shown in Figs. 6(*a*) and (*b*), closely resemble the results of the *NBEAM-MTRX* calculations, shown in Fig. 5. With $\mathbf{P} = (0.43, 0, \pm 0.90)$ and convolution with a Gaussian instrumental function ($\sigma =$ 0.007°), the theory is in good agreement with the experimental results, as shown by the solid curves in Fig. 6.

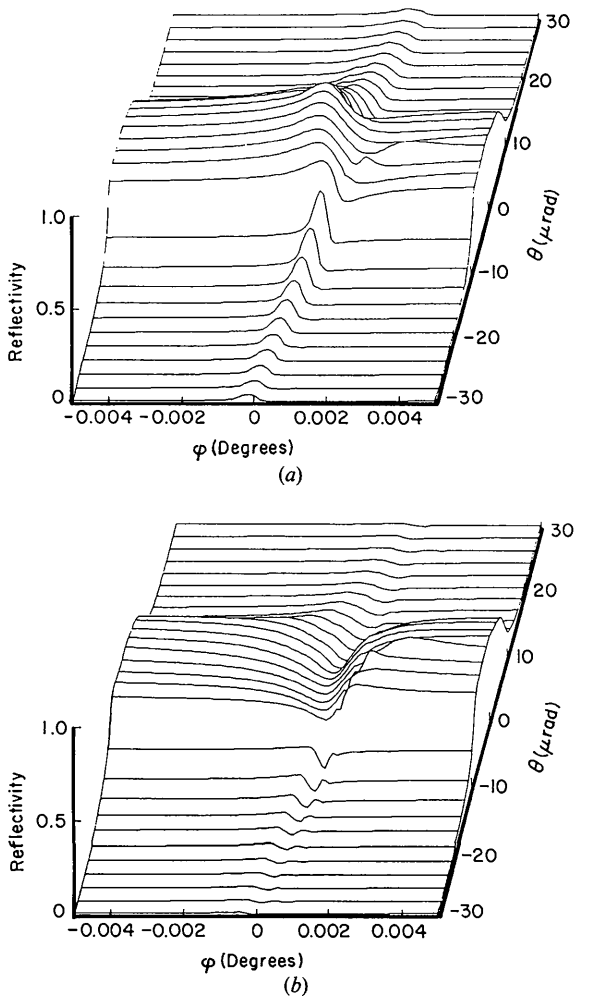

Fig. 4. Calculated reflectivity of the Ge 333/13$\bar{3}$ reflection as a function of rocking angle θ and azimuthal angle φ. The incident polarization used in the calculation is (*a*) $\mathbf{P} = (0, 0, 1)$ and (*b*) $\mathbf{P} = (0, 0, -1)$. The definitions of the zero points on both the θ and φ axes are arbitrary.

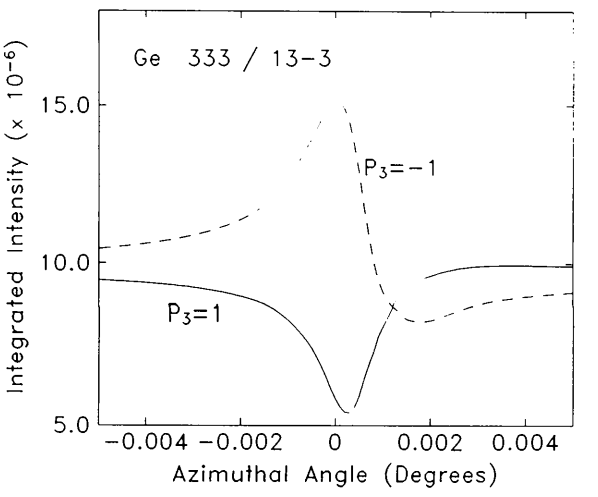

Fig. 5. Calculated integrated intensities as a function of azimuthal angle φ for the Ge 333/13$\bar{3}$ reflection. The incident polarization is $\mathbf{P} = (0, 0, 1)$ for the solid curve and $\mathbf{P} = (0, 0, -1)$ for the dashed curve. The definition of the zero point on the φ axis is arbitrary.

Both the Ge 333 and the GaAs 442 series can be used as circular polarization analyzers. The Ge 333 has the advantage of high reflectivity but requires a highly collimated beam. The GaAs 442 has a lower reflectivity but can tolerate a moderate angular divergence in the incident beam. The choice of the two types, strong or weak main reflection, will be dependent on specific experimental conditions.

3. *X-ray phase plate: circular polarizer*

Creating circularly polarized X-ray beams by crystal optics has attracted great interest in recent years. Using the effect of birefringence within a Bragg reflection, Mills (1988) demonstrated that the Laue transmitted beam can be circularly polarized if the crystal thickness is correct for the X-ray wavelength. Hirano, Izumi, Ishikawa, Annaka & Kikuta (1991) showed the same effect on the tails of a reflection by using the Bragg transmitted beam. It was shown by Brümmer, Eisenschmidt & Höche (1984) and more recently by Batterman (1992) that, by using multiple bounces, circular polarization can be achieved also on a Bragg reflected beam.

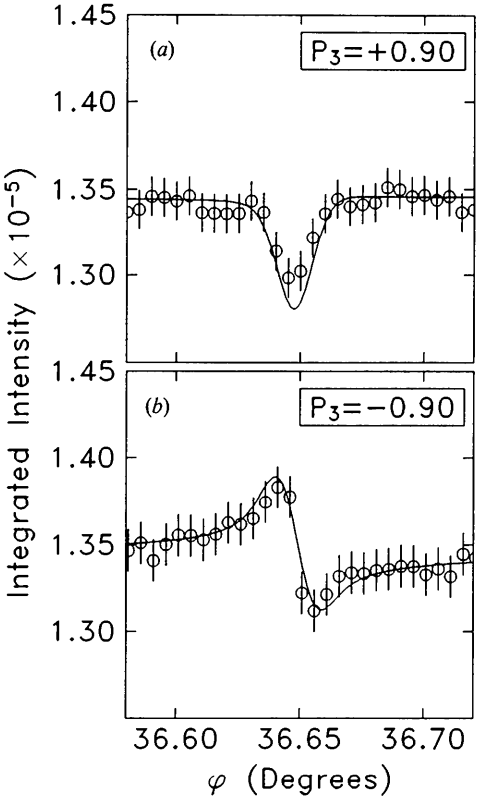

Fig. 6. Three-beam intensity profiles of the Ge 333/13$\bar{3}$ reflection. The experimental results (open circles) are obtained using elliptically polarized synchrotron radiation (*a*) above and (*b*) below the orbital plane. The error bars correspond to three times the standard deviation of accumulated counts at each φ position. The solid curves are three-beam dynamical calculations using incident polarization of (*a*) $\mathbf{P}=(0.43, 0, 0.90)$ and (*b*) $\mathbf{P}=(0.43, 0, -0.90)$. These polarization parameters are derived from the synchrotron-radiation properties and the experimental set-up. The azimuthal-angle origin is defined by the convention that the reciprocal vector (0, 1, −1) is lying on the diffraction plane with a projection that is antiparallel to the incident wave vector $\mathbf{k}_0$. The surface normal of the crystal is assumed to be along the [111] direction.

A new way of making an X-ray circular phase plate is to use multibeam diffraction since this can turn a linearly polarized incident beam into one with circular or elliptical polarization. The reason is simple. First, we know that a multiple-beam diffraction process can provide a π-polarization component from a pure σ-polarized incident beam. Second, the π component from the multibeam process can have a phase shift, $\delta+\nu(\varphi)$, relative to the σ diffracted wave of the main reflection. The combination of these two effects will naturally give rise to an elliptically polarized X-ray beam.

With (3), it is straightforward to show that the Poincaré polarization components $\mathbf{P}'=(P_1', P_2', P_3')$ of the diffracted beam are given by

$$\begin{aligned} P_1' &= (\rho_{11}'-\rho_{22}')/I, \\ P_2' &= (\rho_{21}'+\rho_{12}')/I, \\ P_3' &= (\rho_{21}'-\rho_{12}')/iI, \end{aligned} \tag{6}$$

where $I=\rho_{11}'+\rho_{22}'$ is the intensity of the diffracted beam. For a multiple-beam diffraction process, once the matrix $\{\mathbf{M}\}$ is calculated through the *NBEAM* program, the polarization components of the diffracted beam are readily obtained using (3) and (6).

An example of the results of such calculations is shown in Fig. 7. The multiple-beam combination is the GaAs 442/151. To be consistent with our first example, we assume the same surface orientation (111) in the calculation. The incident beam is assumed to be purely σ polarized: $\mathbf{P}=(1, 0, 0)$. In Fig. 7, we show the calculated circular component P_3' in the diffracted beam as functions of azimuthal angle φ and rocking angle θ. The plot shows that a significant portion of the diffracted beam is circularly polarized, with a maximum P_3' of $\pm 60\%$ at the center of the rocking curve and near the multiple-beam excitation. Since the 442 rocking-curve width is only a few μrad wide, a more realistic way of visualizing the effect is to use the θ-integrated $\bar{\mathbf{P}}'$, which is defined by taking a reflectivity[$R(\theta)$]-weighted average at a given φ:

$$\mathbf{P}'=\sum_i R(\theta_i)\mathbf{P}'(\theta_i)/\sum_i R(\theta_i).$$

The three components of $\bar{\mathbf{P}}'$ are shown in Fig. 8, along with the θ-integrated intensity, as a function of azimuthal angle φ.

Let us examine more closely what happens to $\bar{\mathbf{P}}'$ when we scan the azimuthal angle through the

multiple-beam reflection. Far away from the three-beam point, the diffracted beam is almost completely horizontally polarized, the same as the incident beam. A small fraction of P_2' exists because of the surface miscut of the crystal. When the three-beam point is approached, a portion of the diffracted beam turns into one of circular polarization P_3', which reaches its maximum at the side of the multiple reflection peak. Within the multiple reflection peak the linear component P_1' continues to drop but is mainly converted to a 45°-tilt linear component P_2', while the circular component P_3' goes through zero and changes its handedness at the other side of the peak. This implies that one can easily flip the handedness of the circular polarization by a small change in azimuthal angle, which is a valuable feature for a phase plate.

This asymmetric line shape of P_3' depends upon the structural phase triplet δ of the multiple reflection and reverses its asymmetry when δ changes its sign. This point can be easily seen from (6) and (3):

$$P_3' = 2M_{\sigma\pi} \sin \delta / I, \tag{7}$$

for $P_1 = 1$ in the incident beam. P_3' does not depend on $M_{\pi\sigma}$ because of the assumption that the incident beam is purely σ polarized. An interesting application of (7) is that one could obtain the *handedness* phase information of a crystal if one analyzed the *circular* component in its multibeam diffracted intensity using *linearly* polarized incident X-rays. This would be an alternative method to the one discussed in the first example, where an incident beam having circular polarization is required.

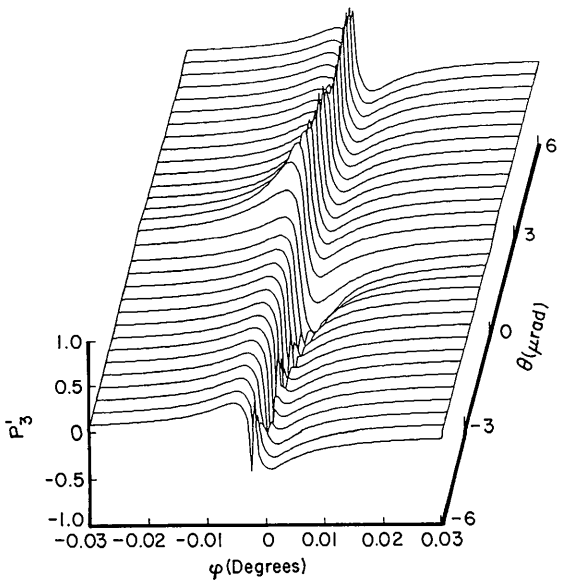

Fig. 7. Calculated scattered circular-polarization component P_3' of the GaAs 442/151 multiple reflection as a function of the rocking angle θ and the azimuthal angle φ. The incident polarization is assumed to be purely σ polarized, $\mathbf{P}=(100)$. The definitions of the zero points on both the θ and φ axes are arbitrary.

Concluding remarks

We have extensively investigated the effect of polarization mixing in a multiple-beam Bragg diffraction, using a new density-matrix formalism in the dynamical theory of N-beam diffraction. We have shown that the combination of the two effects, polarization mixing and multibeam interference, can provide several new and interesting applications of N-beam diffraction. First, using an elliptically polarized X-ray beam it is possible to obtain acentric phase information from the asymmetric profile of a multiple-reflection peak. This would enable one to determine the handedness or polarity of a noncentrosymmetric crystal. Second, for a known crystal structure, the same intensity profile can be used to measure circular

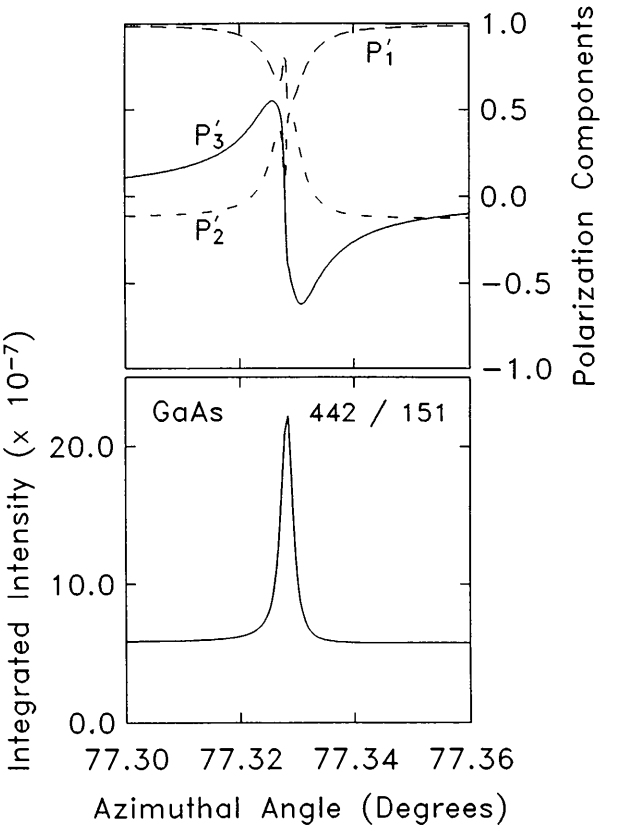

Fig. 8. The top plot shows the calculated results of the integrated scattered polarization components $\bar{\mathbf{P}}' = (P_1', P_2', P_3')$ *versus* the azimuthal angle φ for the GaAs 422/151 multiple reflection with a completely σ-polarized incident beam, $\mathbf{P}=(100)$. The integrated intensities are shown in the lower plot. The azimuthal-angle origin is defined by the convention that the reciprocal vector $(-1, 1, 0)$ is lying on the diffraction plane, with a projection that is antiparallel to the incident wave vector $\mathbf{k}_0$. The surface normal of the crystal is assumed to be along the [111] direction.

polarization in the incident beam. For this purpose we have shown that the intensity profile within the multiple-reflection peak for a centrosymmetric crystal such as germanium can be used. Third, *N*-beam diffraction can produce circularly or elliptically polarized X-rays from a linear incident polarization and therefore can be used as an X-ray phase plate. With greater availability of synchrotron-radiation sources worldwide, it is our belief that the technique of multiple-beam diffraction will find more use, both in X-ray physics and crystallography and in synchrotron-radiation instrumentation.

The author is grateful to K. D. Finkelstein and B. W. Batterman for many stimulating discussions. This work is supported by the United States National Science Foundation, through CHESS, under Grant No. DMR 90-21700.

References

BATTERMAN, B. W. (1992). *Phys. Rev. B*, **45**, 12677-12681.

BATTERMAN, B. W. & COLE, H. (1964). *Rev. Mod. Phys.* **36**, 681-717.

BEDZYK, M. J. & MATERLIK, G. (1985). *Phys. Rev. B*, **32**, 6456-6463.

BELYAKOV, V. A. & DMITRIENKO, V. A. (1989). *Sov. Phys. Usp.* **32**, 697-719.

BLUME, M. & GIBBS, D. (1988). *Phys. Rev. B*, **37**, 1779-1789.

BORN, M. & WOLF, E. (1983). In *Principles of Optics*, 6th ed. New York: Pergamon.

BRÜMMER, O., EISENSCHMIDT, CH. & HÖCHE, H. R. (1984). *Acta Cryst.* A**40**, 394-396.

CHANG, S. L. (1982). *Phys. Rev. Lett.* **48**, 163-166.

CHANG, S. L. & TANG, M. T. (1988). *Acta Cryst.* A**44**, 1065-1072.

CHAPMAN, L. D., YODER, D. R. & COLELLA, R. (1981). *Phys. Rev. Lett.* **46**, 1578-1581.

COLE, G., CHAMBERS, F. W. & DUNN, H. M. (1962). *Acta Cryst.* **15**, 138-144.

COLELLA, R. (1974). *Acta Cryst.* A**30**, 413-423.

FINKELSTEIN, K. D., SHEN, Q. & SHASTRI, S. (1992). *Phys. Rev. Lett.* **69**, 1612-1615.

HIRANO, K., IZUMI, K., ISHIKAWA, T., ANNAKA, S. & KIKUTA, S. (1991). *Jpn. J. Appl. Phys.* **30**, *L*407-*L*409.

HUMMER, K. & BILLY, H. W. (1986). *Acta Cryst.* A**42**, 127-133.

HUMMER, K., WECKERT, E. & BONDZA, H. (1989). *Acta Cryst.* A**45**, 182-187.

JACKSON, J. D. (1975). *Classical Electrodynamics.* New York: Wiley.

JURETSCHKE, H. J. (1982). *Phys. Rev. Lett.* **48**, 1487-1489.

KIRFEL, A., PETCOV, A. & EICHHORN, K. (1991). *Acta Cryst.* A**47**, 180-195.

MILLS, D. M. (1988). *Nucl. Instrum. Meth. Phys. Res.* A**266**, 531-534.

MOON, R. M. & SHULL, C. G. (1964). *Acta Cryst.* **17**, 805-812.

POST, B. (1977). *Phys. Rev. Lett.* **39**, 760-763.

RENNINGER, M. Z. (1937). *Z. Phys.* **106**, 141-176.

SHEN, Q. (1986). *Acta Cryst.* A**42**, 525-533.

SHEN, Q. (1991). *Proc. Soc. Photo Opt. Instrum. Eng.* **1550**, 27-33.

SHEN, Q. & COLELLA, R. (1986). *Acta Cryst.* A**42**, 533-538.

SHEN, Q. & COLELLA, R. (1987). *Nature (London)*, **329**, 232-233.

SHEN, Q. & COLELLA, R. (1988). *Acta Cryst.* A**44**, 17-21.

SHEN, Q. & FINKELSTEIN, K. D. (1990). *Phys. Rev. Lett.* **65**, 3337-3340.

SHEN, Q. & FINKELSTEIN, K. D. (1992). *Phys. Rev. B*, **45**, 5075-5078.

TEMPLETON, D. H. & TEMPLETON, L. K. (1985). *Acta Cryst.* A**41**, 133-142.

WARREN, B. E. (1969). *X-ray Diffraction.* New York: Addison-Wesley.

ZACHARIASEN, W. H. (1965). *Acta Cryst.* **18**, 705-710.

Acta Cryst. (1993). A**49**, 613–623

A Mathematical Model for the Stacking Patterns of Planar Copper(II) Halide Oligomers

BY ROGER D. WILLETT

Department of Chemistry and Program in Materials Science, Washington State University, Pullman, WA 99164, USA

(*Received* 17 *August* 1992; *accepted* 11 *January* 1993)

Abstract

Planar bibridged $Cu_nX_{2n}L_2$ oligomers, where X is a halide ion and L a halide ion or neutral ligand, with values of n ranging from 1 to 7, occur in numerous copper(II) halides. Within the oligomers, each Cu^{II} ion assumes an approximate square-planar primary coordination geometry. Common examples include $Cu_2X_6^{2-}$, $Cu_3X_8^{2-}$ and $Cu_4X_{10}^{2-}$ anions and neutral species such as $[CuCl_2(H_2O)_2]$, $[Cu_2Br_4(pyridine)_2]$ and $[Cu_3Cl_6(CH_3CN)_2]$. The oligomers aggregate through the formation of long semicoordinate Cu–X linkages, creating stacks of oligomers. A wide variety of stacking arrangements (polytypes) is possible, corresponding to different sequences of relative translations between adjacent oligomers. The ground states of a one-dimensional Hamiltonian are developed to account for a subset of the observed polytypism. Terms included in the Hamiltonian include quadratic $(\mathbf{S}_i \cdot \mathbf{S}_j)$ nearest- and next-nearest-neighbor interactions, nearest-neighbor biquadratic $[(\mathbf{S}_i \cdot \mathbf{S}_j)^2]$ interactions and nearest-neighbor XY-interaction